Nickel superoxide dismutase: Structural and functional roles of Cys2 and Cys6

ARTICLE *in* EUROPEAN JOURNAL OF BIOCHEMISTRY · MARCH 2010

Impact Factor: 2.54 · DOI: 10.1007/s00775-010-0645-y · Source: PubMed

5 AUTHORS, INCLUDING:

Diane E Cabelli
Brookhaven National Laboratory
99 PUBLICATIONS **3,128** CITATIONS
SEE PROFILE

Thomas C Brunold
University of Wisconsin–Madison
102 PUBLICATIONS **3,909** CITATIONS
SEE PROFILE

Michael J Maroney
University of Massachusetts Amherst
117 PUBLICATIONS **3,485** CITATIONS
SEE PROFILE

Published in final edited form as:
J Biol Inorg Chem. 2010 June ; 15(5): 795–807. doi:10.1007/s00775-010-0645-y.

Nickel Superoxide Dismutase: Structural and Functional Roles of Cys2 and Cys6

Kelly C. Ryan[1], **Olivia E. Johnson**[2], **Diane E. Cabelli**[3], **Thomas C. Brunold**[2], and **Michael J. Maroney**[1]

Michael J. Maroney: mmaroney@chemistry.umass.edu

[1] Department of Chemistry, University of Massachusetts at Amherst, 104 Lederle Graduate Research Tower A, 710 North Pleasant Street, Amherst, MA 01003, Phone: 413-545-4876, Fax: 413-545-4490

[2] Department of Chemistry, University of Wisconsin-Madison, 1101 University Avenue, Madison, WI 53706

[3] Department of Chemistry, Building 555A Brookhaven National Laboratory, P.O. Box 5000, Upton, NY 11973

Abstract

Nickel superoxide dismutase (NiSOD) is unique among the family of SOD enzymes in that it coordinates cysteine residues (Cys2 and Cys6) to the redox-active metal center and exhibits a hexameric quaternary structure. To assess the role of the Cys residues with respect to the activity of NiSOD, mutations of Cys2 and Cys6 to serine (C2S-, C6S-, and C2S/C6S-NiSOD) were carried out. The resulting mutants do not catalyze the disproportionation of superoxide, but retain the hexameric structure found for wild-type (WT) NiSOD and bind Ni(II) ions in a 1:1 stoichiometry. X-ray absorption spectroscopic (XAS) studies of the Cys mutants reveal that the nickel active-site structure for each mutant resembles that of C2S/C6S-NiSOD and demonstrate that mutation of either Cys2 or Cys6 inhibits coordination of the remaining Cys residue. Mutation of one or both Cys residue(s) in NiSOD induces the conversion of the low-spin Ni(II) site in the native enzyme to a high-spin Ni(II) center in the mutants. This result that indicates that coordination of both Cys residues is required to generate the native low-spin configurations and maintain catalytic activity. Analysis of the quaternary structure of the cysteine mutants by differential scanning calorimetry, mass spectrometry, and size-exclusion chromatography reveal that the cysteine ligands, particularly Cys2, are also important for stabilizing the hexameric quaternary structure of the native enzyme.

Keywords

superoxide dismutase (SOD); x-ray absorption spectroscopy (XAS); differential scanning calorimetry (DSC)

Introduction

Superoxide dismutases (SODs) are a family of metalloenzymes that protect aerobic organisms from oxidative stress imposed by the superoxide anion radical ($O_2^{\bullet -}$). Specifically, they catalyze the disproportionation of superoxide to molecular oxygen (O_2) and hydrogen peroxide (H_2O_2) at rates that are at or near the diffusion limit. Therefore, SODs are the first line of defense against this harmful anion [1–4]. During catalysis the redox-active metal cofactor cycles between oxidized and reduced states that differ by one electron (Equations 1–3).

$$M^{(n+1)}+O_2^{\bullet-} \rightarrow M^{n+}+O_2 \quad (1)$$

$$M^{n+}+O_2^{\bullet-}+2H^+ \rightarrow M^{(n+1)}+H_2O_2 \quad (2)$$

$$2O_2^{\bullet-}+2H^+ \rightarrow O_2+H_2O_2 \quad (3)$$

Three classes of SODs exist based on amino acid sequence homology [5–8]: CuZnSOD, FeSOD and MnSOD, and NiSOD. Much like the Fe- and MnSODs, the more recently discovered NiSOD enzyme catalyzes the diproportionation of $O_2^{\bullet-}$ by cycling between M(III) and M(II) oxidation states. Within the SOD family, however, NiSOD is quite unique. For example, nickel is the only metal that does not catalyze $O_2^{\bullet-}$ disproportionation in neutral aqueous solution (in the absence of the protein), presumably because it lacks an accessible one-electron redox process [1,9]. In fact, the Ni(III/II) redox potential for $Ni(OH_2)_6^{2+}$ is estimated to lie at >2V and, thus, well outside the acceptable range for catalyzing the oxidation and reduction of superoxide (*ca.* −160 to +879 mV vs NHE at pH 7) [10]. To overcome this deficiency, NiSOD coordinates active-site residues not found in other SODs. The CuZnSOD, FeSOD, and MnSOD proteins bind their respective catalytic metal cofactors with only N/O-donors. For Fe- and MnSODs the active-site environments include three histidine (His) residues, one aspartate (Asp) side chain, and a H_2O/OH^- ligand, whereas the Cu center in CuZnSOD is ligated by three imidazole ligands, an imidazolate, and a water molecule [11–14]. Alternatively, in NiSOD, which is an 80 kDa homohexamer containing one nickel cofactor per monomer, the nickel center coordinates cis-cysteinate ligands (Cys2 and Cys6) [15,16]. In the reduced state, the Ni(II) cofactor adopts a square planar getometry by also coordinating the N-terminal amine and a deprotonated amide from the Cys2 backbone. In the oxidized state of NiSOD, Ni(III) ion additionally binds the imidazole side chain of His1, which results in a square pyramidal geometry around the nickel ion (Figure 1).

While NiSOD is the only known SOD to contain S-donor ligands in the active site, cysteinate ligation is a recurring theme in the redox biochemistry of nickel proteins. Currently eight nickel-containing enzymes have been crystallized, five of which contain S-donors and feature redox-active nickel sites, (NiSOD [15,16], acetyl coenzyme A synthase (ACS) [17,18], carbon monoxide dehydrogenase (COdH) [19], hydrogenase (H_2ase) [20], and methyl coenzyme M reductase (MCR) [21]). The remaining three enzymes (urease [22], glyoxalase I (Glx1) [23], and acireductone dehydrogenase (ARD) [24,25]) lack S-donors and feature redox-inactive nickel centers. From this observation, it has been proposed that active-site Cys residues are critical for tuning the redox properties of nickel cofactors. Recent density function theory (DFT) calculations on NiSOD active-site models, both in the reduced and oxidized forms, support this hypothesis[26–28].

Regardless of the differences in structure and metal cofactor among the different classes of SODs, similar roles are played by the protein matrices. These roles include adjusting the redox potential of the active site metal ion into the optimum range (~300mV vs. NHE) for the oxidation and reduction of superoxide (Equations 1–3) [29–32], providing the protons necessary for the production of hydrogen peroxide (Equation 2)[33, 34], and controlling access of substrate to the active site [32, 35–38]. Each of these roles may be contingent on the presence of Cys residues at the NiSOD active site. In addition to affecting the NiSOD

redox-activity, the Cys thiolates have been proposed to function in proton transfer, alone or in concert with other second-sphere residues [27, 28]. The active-site Cys residues are also likely to influence the molecular mechanism of NiSOD catalysis. Metal-thiolate bonds are highly susceptible to sulfur-based modifications by strong oxidants such as superoxide and hydrogen peroxide [39–42]; yet, the cysteinate ligands of NiSOD are not oxidized during catalysis. While outer-sphere binding of substrate would seemingly accommodate the unique active-site environment of NiSOD, inner-sphere binding has also been suggested [15, 16, 27].

In this study we have performed mutations of either or both NiSOD active-site S-donors, Cys2 and Cys6, to serine (Ser) (C2S-, C6S-, C2S/C6S-NiSOD) in order to explore their roles with respect to the catalytic activity of NiSOD, and to specifically assess if a single Cys residue would support the redox activity of the nickel site. In addition to providing further evidence for the prerequisite of thiolate ligation in creating redox-active metal center in Nickel enzymes, these studies indicate that *both* thiolate donors are required in order to produce the redox-active nickel site found in NiSOD, and that Cys2 is particularly important for stabilizing the hexameric quaternary structure of the native enzyme.

Materials and methods

Site-Directed Mutagenesis

The single Cys → Ser mutants were prepared by polymerase chain reaction (PCR) of WT-*Streptomyces coelicolor* NiSOD gene with a mutagenic 5′-primer and 3′SODNU and the double Cys → Ser mutant was prepared by PCR of the C6S-NiSOD gene with mutagenic 5′-primer and 3′SODNU (Table 1). The PCR product was gel purified (1% agarose) and treated with T4 DNA polymerase to create overhangs complementary to the Ligation Independent Cloning (LIC) vector pET30 Xa/LIC (Novagen™). The insert was annealed to the vector and NovaBlue (Novagen™) competent cells were transformed with the pET30 Xa/LIC plasmid containing the *sodN* mutant gene for selection. The plasmid containing mutagenic *sodN* was isolated using plasmid mini prep kit from Qiagen and DNA sequencing was performed to confirm the expected base sequence for each mutant (University of Massachusetts-Amherst DNA sequencing facility). BL21 (DE3) pLysS (Novagen™) competent cells were transformed with the plasmid containing the desired mutation(s).

Expression, Purification, Processing, and Reconstitution of C2S-, C6S-, and C2S/C6S-NiSOD proteins

The mutant proteins were expressed and purified as previously reported[43]. Single colonies were grown overnight at 37°C with shaking in 10 mL Luria-Bertani broth, supplemented with chloramphenicol (cam) and kanamycin (kan) for selection. These cultures were added to 1L pre-warmed fresh media and grown to an OD_{600} of 0.6 and then induced with 0.8 mM isopropyl β-D-1-thiogalactopyranoside (IPTG) for 3–5 hours. Cells were harvested by centrifugation, resuspended in 40 mL Ni-NTA binding buffer (10 mM imidazole, 50 mM sodium phosphate, 300 mM sodium chloride pH 8.0), and then frozen at −80 °C to lyse the cells. The cell harvests were thawed and treated with 100 μL of DNAse I solution (10 mg/ml DNAse I, 10 mM magnesium chloride, 20 mM Tris pH 7.5, 40% glycerol) at 37 °C until the viscosity of the solution was significantly reduced. The cell lysate was centrifuged for 5 min at 8,000 rpm and the supernatant was used for protein purification.

All chromatographic purifications employed an AKTA-FPLC (Amersham Biosciences). The cell lysate supernatant was loaded onto a column (Pharmacia HR10) containing Ni-NTA HisBind Superflow™ resin (Novagen™) at 3 ml/min with Ni-NTA binding buffer. Once the absorbance at 280 nm returned to the baseline, the buffer was changed to 33% elute buffer

(250 mM imidazole, 50 mM sodium phosphate, 300 mM sodium chloride pH 8.0) in one step, and the column was washed with 7 column volumes of 33% elute buffer. The fusion protein was then eluted from the column using 100% elute buffer. Electrospray ionization mass spectroscopy (ESI-MS) was used to confirm the molecular weight (MW) of the expected fusion protein (*vide infra*).

The purified fusion protein was cleaved to yield NiSOD with the WT N-terminus by using Factor Xa. The fusion protein was buffer exchanged three times with 20 mM Tris buffer pH 8.5 and then seven times with Factor Xa cleavage buffer (5 mM calcium chloride, 50 mM Tris, 100 mM sodium chloride, pH 8.0) in an argon pressure concentrator outfitted with a 10 kDa molecular weight cut off (MWCO) Millipore ultrafiltration membrane. The concentration of fusion protein in Factor Xa cleavage buffer was determined using a bicinchoninic acid (BCA) assay. The assay was performed using the Enhanced Test Tube Protocol outlined in Pierce's BCA™ Protein Assay Kit instruction manual. Factor Xa was then added (1 unit/50 μg fusion protein) and the mixture was incubated at 4 °C. The extent of cleavage was monitored using 14% SDS-PAGE. Processed protein was reduced with a five-fold excess dithiothreitol (DTT) and reconstituted with a three-fold excess $NiCl_2$ in an anaerobic glove box (Coy Laboratory Products, Inc.).

ESI-MS Analysis

To determine the MW of the expression products, ESI-MS analysis was performed using a Bruker Esquire mass spectrometer on solutions of denatured proteins (final concentration of 5 mM monomer) in a 10 mM aqueous ammonium acetate solution with 3% acetic acid and 50% MeOH (Table 2). To determine the oligomeric state of the proteins, ESI-MS was also performed under non-denaturing conditions on a JMS-700 MStation magnetic sector (double focusing) mass spectrometer. The orifice voltage was turned to 0 V and the skimmer voltage was set to 120 V to prevent oligomeric breakdown. Under these conditions, WT-NiSOD exhibits a spectrum that arises from hexameric holo-NiSOD [35]. Spectra were obtained from solutions of 60 μM NiSOD (monomer) in 10 mM ammonium acetate.

Metal Analysis

A PerkinElmer Optima 4300 DV inductively coupled plasma-optical emission spectrometer (ICP-OES) was used to quantify the nickel content of the reconstituted mutant proteins. This instrument is equipped with a 40 MHz free-running generator and a segmented-array charge-coupled device (SCD) detector. The sample introduction system consisted of a concentric nebulizer with a cyclonic spray chamber. The concentration of nickel in each sample was determined at $\lambda = 231.604$ nm.

Quaternary Structure and Stability

Size-exclusion chromatography was performed using a Superdex 75 15/300 GL (GE lifesciences) column. The column was standardized with albumin (67 kDa), ovalbumin (43 kDa), chymotrypsinogen (25 kDa), and ribonuclease A (13.7 kDa). A standard curve was constructed by plotting V_e/V_0 vs MW (where V_e = elution volume of the peak, and V_0 = elution volume of blue dextran), and the data was fit with a second order polynomial. Cys mutants were injected onto the column at a concentration of 480 μM (monomer) in 20 mM Tris, 100 mM NaCl pH 8.0, and the retention volume of the peak(s) (V_e/V_0) from each chromatogram were analyzed using the standard curve to determine the molecular weights of the eluted proteins (see Figure 6 inset)

Melting temperatures (T_m) were measured with a Microcal VP-DSC with a 0.5 mL sample and reference cells. Samples were concentrated to 100–140 μM monomer in 50 mM Tris buffer. Protein samples and blank 50 mM Tris buffer were degassed under vacuum for 10

min and syringed into the cells using a pulsing motion to expel air bubbles. Samples were run at 30 psi over 25–100 °C at a scan rate of 30 °C/hour. Baseline correction and normalization were performed with the Microcal interface to the Origin graphing program, and T_m(s) were taken to be the peak maxima of the thermogram.

X-Ray Absorption Spectroscopy

X-ray absorption spectroscopy (XAS) data collection and analysis were performed as previously described [44]. Nickel *K*-edge XAS data were collected on beamline X9B at the National Synchrotron Light Source (Brookhaven National Laboratory). Samples of frozen protein solutions (1–3 mM, based on nickel content, in 20 mM Tris·HCl, pH 8.0) were placed in polycarbonate holders inserted into aluminum blocks and held near 50 K using a He displex cryostat. The ring conditions for data collection were 2.8 GeV and 120–300 mA. A sagittally focusing Si(111) double crystal monochromator and a 13-channel Ge fluorescence detector (Canberra) were used for data collection. X-ray absorption near-edge spectroscopy (XANES) data were collected from ± 200 eV relative to the nickel *K*-edge. The edge energy reported was taken to be the maximum of the first-derivative of the XANES spectrum. Extended X-ray absorption fine structure (EXAFS) was collected to 9307 eV (k = 16 Å^{-1}). The X-ray energy for the *K*-edge of nickel was internally calibrated to 8331.6 eV using transmission data from a nickel foil. The data shown are the average of 5–6 scans and were analyzed using the EXAFS123 software package [45] for XANES data and the SixPack software package [46] was used for EXAFS analysis. Scattering parameters for SixPack fitting were generated using the FEFF 8 software package [47]. The SixPack fitting software builds on the ifeffit engine and uses iterative FEFF calculations to fit EXAFS data during model refinement, and is thus an improvement over previous methods that employ a static set of calculated scattering parameters. The coordinates of the five coordinate C2S/C6S-NiSOD model obtained from density functional theory geometry optimizations [48] were used as input files for FEFF 8. Two sets of input files were used, one that included all non-hydrogen atoms from the calculation, and another which eliminated the carbon and nitrogen atoms contributed by the apical imidazole ligand. Comparison of the fits obtained using these two models was used to assess ligation by the side chain of His1. To compare different models to the same data set, ifeffit uses three goodness of fit parameters, χ^2 (Equation 4), reduced χ^2, and the *R*-factor (Equation 5), where N_{idp} is the number of independent data points, N_{ε^2} is the number of uncertainties to minimize, Re(f_i) is the real part of the EXAFS fitting function, and Im(f_i) is the imaginary part of the EXAFS fitting function. Reduced $\chi^2 = \chi^2/(N_{ind}\, N_{varys})$ (where N_{varys} is the number of refining parameters) and represents the degrees of freedom in the fit.

$$\chi^2 = \frac{N_{idp}}{N_{\varepsilon^2}} \sum_{i=1}^{N} \left\{ [\mathrm{Re}(f_i)]^2 + [\mathrm{Im}(f_i)]^2 \right\} \tag{4}$$

Ifeffit also calculates the *R*-factor for the fit, which is given by Equation 5 and is scaled to the magnitude of the data, making it proportional to χ^2. To compare different models (fits) the *R*-factor and reduced χ^2 parameters can be evaluated to determine which model provides the best fit, in which case both parameters should be minimized. Although the *R*-factor will always improve with an increasing number of adjustable parameters, reduced χ^2 will go through a minimum and then increase, indicating that the model is over fitting the data.

$$R=\frac{\sum_{i=1}^{N}\left\{[\mathrm{Re}(f_i)]^2+[\mathrm{Im}(f_i)]^2\right\}}{\sum_{i=1}^{N}\left\{[\mathrm{Re}(\tilde{\chi}\ data_i)]^2+[\mathrm{Im}(\tilde{\chi}\ data_i)]^2\right\}} \quad (5)$$

Pulse Radiolysis

The pulse radiolysis experiments were carried out using a 2 MeV van de Graaff accelerator at Brookhaven National Laboratory. Superoxide radicals were generated upon pulse radiolysis of an aqueous, air/O_2 saturated solution containing 10 mM phosphate, 30 mM formate, and 5 μM ethylenediaminetetraacetic acid (EDTA) (Equations 6–10).

$$OH+HCO_2^- \rightarrow H_2O+CO_2^{\bullet-} \quad (6)$$

$$CO_2^{\bullet-}+O_2 \rightarrow CO_2+O_2^{\bullet-} \quad (7)$$

$$e_{aq}^-+O_2 \rightarrow O_2^{\bullet-} \quad (8)$$

$$H^{\bullet}+O_2 \rightarrow HO_2^{\bullet} \quad (9)$$

$$HO_2 \rightarrow O_2^{\bullet-}+H^+ \quad (10)$$

Catalytic rate constants were obtained by monitoring the disappearance of $O_2^{\bullet-}$ at 260 nm in the presence of micromolar concentrations of mutant NiSOD. The path length of the quartz cell used was 2.0 cm and a 100–700 ns pulse width was chosen, resulting in the generation of 1–7 μM $O_2^{\bullet-}$ per pulse. The reported rate constants are based on metal concentration, with the assumption that all nickel ions are specifically bound and equally contributing to $O_2^{\bullet-}$ dismutation.

Results

Protein Characterization—All of the expressed fusion proteins had the MWs expected for the amino acid single and double substitutions intended (Table 2). Upon reconstitution of proteins processed to remove the N-terminal extension, each of the mutants bound nickel at close to stoichiometric 1:1 ratios (Table 2). Unlike the native enzyme, which is golden-brown in color, all of the Cys → Ser NiSOD mutants are colored Kelly green. This color change results from the loss of the transition near 380 nm that is assigned to a S → Ni(III) charge transfer (CT) transition in the WT enzyme [26], and the appearance of a new ligand-field transition near 420 nm (note electronic structures of the Cys → Ser NiSOD mutants are discussed in detail in the accompanying article [48]). Size-exclusion chromatography showed that the expressed fusion protein, the processed apo-enzyme, holo-NiSOD, and all

of the reconstituted NiSOD mutants give rise to an elution peak with a retention volume corresponding to the molecular weights appropriate for homohexamers (Table 3, Figure 6, and supporting information Figure SI-3). For C6S-NiSOD, only one elution peak was observed, similar to that of holo-WT-NiSOD, which exhibits a small peak to the low retention volume side of the main that is due to a small amount of unprocessed fusion protein in the sample. The chromatogram associated with C2S-NiSOD displayed a second peak with a retention volume consistent with a tetramer (apparent MW = 49.3 kDa). The chromatogram of C2S/C6S-NiSOD exhibited peaks with retention volumes consistent with a mixture of hexameric, tetrameric, and trimeric proteins, with apparent MWs of 77.8, 47.3, and 32.5, kDa respectively. These data indicate that the Cys → Ser mutations cause a destabilization of the quaternary structure of NiSOD, particularly for those involving mutation of Cys2.

The protein thermal stability was also drastically altered by mutations of Cys2 in the C2S- and C2S/C6S-NiSOD mutants, as revealed by the DSC data, melting temperatures (T_m), and stability of the hexamer (Table 2). The DSC thermogram of WT-NiSOD exhibits an asymmetric curve suggesting a complex thermal denaturation of the protein (see Supporting Information). The thermogram associated with the C6S-NiSOD mutant is similar in general appearance to that of WT-NiSOD, but reveals a lower overall melting temperature. In the case of C2S-NiSOD, a second melting transition becomes more resolved, and this is fully resolved in the C2S/C6S-NiSOD profile (Figure 2). These data suggest that the complex denaturation of NiSOD becomes a two-step unfolding process in the C2S- and C2S/C6S-NiSOD.

The decreased hexamer stability of the Cys → Ser mutants is also evident from the ESI-MS data obtained under non-denaturing conditions. WT-NiSOD displays an envelope in the 4000–5000 m/z region corresponding to the homohexameric quaternary structure, and small envelopes in the range of 500–2000 m/z suggesting traces of monomer and trimer in the gas phase. The ESI-MS data obtained under the same conditions for the Cys → Ser mutants display an increased amount of monomer and/or trimer oligomeric states as compared to WT-NiSOD. The spectrum of C6S-NiSOD, whose thermal melting profile most closely resembles that of WT-NiSOD, contains a major envelope corresponding to hexamer. However, compared to WT-NiSOD a more significant monomer envelope is observed. The spectra of the C2S- and C2S/C6S-NiSOD mutants contain a significant monomer envelope and very little intensity in the region associated with the hexamer.

Electron Paramagnetic Resonance—Substitution of cysteine with serine dramatically affects the electronic properties of the nickel center. EPR spectroscopy was used to characterize the redox state of the nickel center in the as-isolated protein. Resting (as-isolated) native and recombinant WT-NiSOD exhibit a rhombic EPR spectrum that arises from a five-coordinate, low-spin ($S = 1/2$) Ni(III) center, with the unpaired electron residing in the Ni dz^2-based molecular orbital [35]. None of the Cys mutants exhibited this EPR spectrum; all were EPR-silent (data not shown), indicating that only Ni(II) was present. Variable-temperature MCD results further indicate that a paramagnetic S = 1 metal center is formed, consistent with the presence of a high-spin Ni(II) ion within the active-site of each mutant [48].

X-ray Absorption Spectroscopy

XANES—The XANES region of the nickel *K*-edge XAS spectrum provides information about the nickel center coordination number and geometry. The spectra obtained for C2S-, C6S-, and C2S/C6S-NiSOD are surprisingly similar and indicate that the nickel sites in all of the Cys mutants have very similar coordination geometries and ligand environments

(Figure 4). The peak areas associated with the feature involving 1s → 3d electronic transitions (Table 3) are consistent with the presence of a five coordinate nickel center in each case.[49] The presence of a shoulder associated with a feature involving a 1s → $4p_z$ electronic transition in all three spectra is consistent with a pyramidal geometry for the nickel sites.[49] Compared to WT-NiSOD, the XANES data for the Cys mutants also feature an increase in the white line region (0–50 Δ eV) that is indicative of an increase in the ratio of N/O-donors to S-donors [49].

EXAFS—The EXAFS region of the XAS spectrum provides information regarding the metal ligands, including the donor-atom types, numbers, and the bond distances. The spectra obtained from samples of C2S- C6S-, C2S/C6S-NiSOD are remarkably similar given that different numbers of potential S-donor ligands are present (Figure 5). Analysis of the EXAFS features arising from atoms in the first coordination sphere indicates that the best fits for the Cys mutants are those with exclusively N/O-donors. The best fit is obtained with five such ligands, consistent with the XANES analysis. The fact that S-donor ligands are absent in all cases indicates that when either one of the Cys-S-donors is mutated to a Ser-O-donor the active site is perturbed such that the other Cys-S-donor is no longer a ligand. This proposal is supported by the UV-vis spectra of the Cys → Ser mutants, which lack the features associated with the CysS → Ni CT transitions observed in the WT-NiSOD spectrum, as well as the fact that the corresponding CD and MCD data that are characteristic of a nickel-binding environment composed of N/O-donor ligands [48].

Multiple-scattering analysis that includes data from scattering atoms in the second and third coordination sphere of the nickel center supports the presence of one imidazole ligand, consistent with nickel binding to His1. Table 4 and Figure 5 compare the best fits obtained for Cys mutants of NiSOD with and without paths derived from imidazole binding (second coordination sphere C and third coordination sphere N and C atoms). These fits also include the main chain carbon atoms from His1 and Cys2, which are involved in five-member chelate rings, and thus held at specific distances that are similar to those involving the second coordination sphere imidazole C atoms. The best fits for the mutants were invariably those that included an imidazole ligand.

Kinetics—The rate of superoxide dismutation by Cys → Ser mutants was determined by monitoring the disappearance of the optical absorbance of pulse radiolytically generated superoxide at 260 nm, in the presence and absence of the NiSODs. The catalytic rate observed for WT-NiSOD at pH 7.5 is 0.71×10^9 $M^{-1}s^{-1}$ [35], as measured by following the first-order disappearance of superoxide that is proportional to the NiSOD concentration. In contrast, in the presence of the Cys mutants, the rate of disappearance of superoxide is no longer first-order but is now second-order and the half-life of superoxide disappearance is now proportional to superoxide concentration. Compared to the spontaneous rate of superoxide dismutation (~2×10^5 $M^{-1}s^{-1}$)[50,51], the Cys mutants show no increase in the rate of disappearance of superoxide (Table 2), and are therefore not catalysts for superoxide disproportionation. WT-NiSOD displays a pH-independent catalytic rate, indicating that the protons required to produce H_2O_2 are derived from the protein rather than bulk solvent [52]. The disappearance of superoxide in the presence of the Cys mutants displayed a pH-dependant rate (slope = −1), indicating that superoxide disappearance is uncatalyzed, where the slope of −1 comes from the lack of reactivity of the superoxide with itself (see Supporting Information).

Discussion

The mutation of the Cys ligands of NiSOD to Ser residues results in proteins that still bind nickel in a 1:1 stoichiometry, have remarkably similar spectroscopic properties, including

the loss of the Ni(III) EPR signal characteristic of the native enzyme, and no longer catalyze the disproportionation of superoxide. This confirms the essential role played by the thiolate ligands in stabilizing Ni(III) and supporting catalysis. In SODs, the protein provides the protons necessary for the oxidative half reaction [33,34] and provides a means for optimizing the redox potential of the active site metal ion [29–32]. The redox adjustments in Fe- and Mn-SODs involve subtle changes in the second coordination sphere of the metals. NiSOD is unique among SODs in that it uses a metal that does not catalyze superoxide disproportionation in neutral aqueous solution [1,9]. Presumably, this is due to the fact that the Ni(III/II) redox potential of $Ni(OH_2)_6^{2+}$ is estimated to lie at > 2V[9] and, thus, well beyond the range of physiologically accessible redox potentials (*ca.* −670 to +816 mV vs. NHE) [53] and outside the limits for SOD catalysis (−160 mV for O_2/O_2^- and +870 mV for O_2^-/H_2O_2 vs. NHE) [10]. Because the NiSOD protein must drastically alter the redox potential of the nickel center to reach the optimum potential near 300 mV, it employs a unique set of ligands that includes two anionic thiolate S-donors from Cys2 and Cys6.

Several DFT calculations have been performed on the active site of NiSOD to investigate the mechanistic roles of the Cys residues. These studies indicate that the S-donor residues Cys2 and Cys6 are crucial in tuning the redox properties of the metal cofactor and serve as a possible source of protons for the oxidative half-reaction [26–28]. From calculations on a Ni(II)SOD active-site model [26], it was proposed that the highly covalent character of the Ni-S_{Cys} bonds derives from σ-bonding interactions[26]. The net non-bonding π-interactions or filled/filled interactions promote Ni(II)-based oxidation over S-based oxidation and assist in redox tuning of the metal center. In addition, Cys2 and/or Cys6 have been implicated to be intimately involved in protonation steps in the catalytic cycle of NiSOD. Calculations indicate that protonation of the Cys side chains in the reduced state of the enzyme has little effect on the Ni-S bond distances [26]. This prediction is supported by structural studies of model compounds that show only small changes in M-S distances upon protonation and alkylation of model compounds [39–42]. In one study, investigation of the solvent-accessible face of the equatorial plane in NiSOD suggested the side chain of Cys2 has more electron density than Cys6. This finding implicates the S-donor of Cys2 as a protonation site for the oxidative half reaction [27]. However, in another study the H-bonding network involving Cys6, Tyr9, and a water molecule was suggested to be the source of protons, indicating that the protonation of Cys6 leads to a thermodynamically favorable proton transfer in the formation of H_2O_2 in NiSOD [28]. The theoretical predictions that the Cys ligands can be protonated in the reduced enzyme are supported by S K-edge XAS studies on enzyme reduced with hydrogen peroxide. Specifically, the XAS spectrum of this species lack the features associated with thiolate ligation and instead exhibits evidence of thiol coordination [54].

The Cys → Ser single mutations studied herein were designed to investigate if one S-donor would be sufficient to produce a redox-active nickel site, and if so, to examine changes in pH dependence of the catalytic activity, and to determine which Cys residue provided the greater redox adjustment. The XAS data indicate that the two single-Cys mutant proteins contain five-coordinate pyramidal nickel sites that lack any S-donor ligand, regardless of which cysteine is mutated. In fact, the two single-Cys mutants have nickel site structures that are essentially identical to that inferred for the double-Cys mutant that lacks both S-donor ligands. The best fits obtained involve 2–3 shells of N/O-scattering atoms in the first coordination sphere (Table 4), including a short, 1.8 Å Ni-N/O distance that is associated with the amidate ligand in WT NiSOD.[35] Features observed from scattering by the atoms in the second and third coordination spheres are consistent with the presence of an imidazole ligand from a His residue. With the WT-crystal structures as a guide[15,16], the structure that emerges from EXAFS and XANES analysis is consistent with retention of the N-terminal His1 amine and the amidate of residue2 in the basal plane, and with the three longer

Ni-N/O distances derived from a combination of the side chains of His1, Ser2 (or Ser6), and solvent.

Six-coordinate Ni(II) complexes are invariably high-spin, and five-coordinate complexes exhibit roughly a 50–50 distribution of high- and low-spin electronic configurations [55]. MCD data show that all of the Cys mutants contain high-spin Ni(II) centers [48]. It was unanticipated that loss of either S-donor ligand would lead to the loss of the second. This change in ligation apparently arises because of a spin-state change in the Ni(II) site. Loss of the remaining thiolate upon conversion to a high-spin complex is consistent with nickel coordination chemistry. Few examples of high-spin Ni(II) thiolates have been characterized [55]. Examples include the tetrahedral $Ni(S\text{-}Ar)_4^{2-}$ anions ($Ni\text{-}S_{Avg}$ = 2.28 Å) [56], five-coordinate trigonal-bipyramidal (Ni-S = 2.26–2.36 Å) [40,57,58], and a few six-coordinate complexes that utilize chelation thiolate ligands and feature very long Ni-S distances (Ni-S = 2.46–2.54 Å)[59] compared to those that are typical of low-spin complexes such as WT-NiSOD (< 2.2 Å) [35]. High-spin Ni(II) monothiolate complexes are exceedingly rare, the only structurally characterized examples being the nickel complex of RcnR, a nickel-responsive transcriptional regulator that features a Ni-S distance of 2.54 Å, and [Ni(tren)(1,3-dtsq)(H_2O or ClO_4) which feature a Ni-S distance of 2.42 and 2.46 respectively [60,61]. The “all or none” requirement for the S-donors in NiSOD therefore indicates that both S-donors are required to support the native low-spin Ni(II) electronic configuration and that loss of either S-donor leads to conversion to a high-spin Ni(II) center and loss of the remaining S-donor ligand.

In addition to producing a redox active nickel site and stabilizing the low-spin electronic structure, the cysteine ligands also play important protein structural roles. The DSC thermograms of the Cys → Ser mutants are significantly different from that of WT-NiSOD (Figure SI-2). For WT-NiSOD, an asymmetric peak with a maximum at 84.8 °C and a broad shoulder centered at ~65 °C is observed. This behavior hints at a complex unfolding process consistent with a slow progression in oligomeric state from hexamer to monomer and subsequent unfolding of the monomeric protein. The thermogram of C6S-NiSOD is similar in shape to that of WT-NiSOD, but the maximum is downshifted by more than 15 °C, indicating that the mutant protein is thermally less stable. The DSC thermogram of C2S-NiSOD begins to show evidence of a two-state unfolding mechanism, which becomes clearly resolved in the C2S/C6S-NiSOD data. The thermogram of double Cys → Ser mutant exhibits two maxima at 53.5 and 81.3 °C. The latter maximum is close to the maximum observed for WT-NiSOD. A likely interpretation of this behavior is that the lower temperature processes correspond to the loss of the hexameric quaternary structure characteristic of NiSOD and that the second process involves unfolding of monomeric subunits. The resolution of the two-step process and retention of a maximum above 80 °C suggests that mutation of Cys2 destabilizes the hexamer, but without dramatically affecting the stability of the monomer.

Data from size-exclusion chromatography and ESI-MS provide additional support for the two-step unfolding mechanism. The size-exclusion chromatogram for C6S-NiSOD shows that hexameric protein is the only species present, whereas for C2S-NiSOD the presence of both hexamers and trimers/tetramers is indicated by two well-defined peaks (Figure 6). When both Cys residues are mutated, a mixture of monomeric, dimeric, trimeric/tetrameric, and hexameric proteins are observed. ESI-MS of WT-NiSOD displays an envelope in the 4000–5000 m/z region corresponding to the homohexameric quaternary structure, and small envelopes in the range of 500–2000 m/z suggesting traces of monomer and trimer in the gas phase. The ESI-MS data obtained under the same conditions for the Cys mutants display an increased amount of monomeric and/or trimeric oligomeric states compared to WT-NiSOD (Figure 3). The spectrum of C6S-NiSOD, which has a DSC profile that most closely

resembles that of WT-NiSOD, contains a prominent envelope corresponding to hexamer. However, compared to WT-NiSOD, a more significant envelope for monomeric protein is also observed. The spectra obtained for C2S-NiSOD and C2S/C6S-NiSOD contain a significant monomer envelope and very little intensity corresponding to the hexamer, consistent with a much less stable hexameric quaternary structure.

Collectively, these data suggest that Cys2 plays a particularly important role in stabilizing the hexameric quaternary structure of the native enzyme. In WT-NiSOD, the Cys2 and Cys6 residues are involved in metal binding: however, several protein contacts are also made with Asp3 and Tyr9 through a water molecule and nearby side chains to form the nickel hook domain. Mutation of Cys2 may well alter the intersubunit interaction between neighboring Asp3 and Lys89, lowering the stability of the hexamer [35].

The apparent effect of metal ligand substitution on the stability of the quaternary structure of the enzyme is unusual, although a similar effect leading to a two-step denaturation and oligomeric destabilization has been documented for the family II pyrophosphatase (family II PPase) from *Bacillus subtilis* [62]. The active site of this enzyme contains two Mn(II) ions coordinated by two His and four Asp residues, plus a water molecule. Additionally, a water molecule and a bidentate Asp ligand bridge the two Mn sites. WT family II PPase forms a dimer where each monomer binds two Mn(II) ions and all metal-binding ligands are derived from the same monomer unit, as in NiSOD. In the absence of metal ions, the thermogram of *B. subtilis* PPase indicates a high degree of cooperativity. This was suggested by a sigmiodal transition in the temperature-induced unfolding measured by circular dichroism (CD). Mutations D13E (binding site one) and D149E (binding site two) resulted in two distinct melting temperatures indicating a two state unfolding mechanism [62].

In summary, the studies of Cys → Ser mutants of NiSOD reveal the essential role of both Cys ligands in the creation of the redox-active nickel center via the supression of the Ni(III/II) redox couple and the stabilization of the low-spin electronic configuration, and also demonstrate that the Ni-hook domain is intimately involved in the stabilization of the hexameric holoenzyme.

Supplementary Material

Refer to Web version on PubMed Central for supplementary material.

Acknowledgments

This work was supported by grants from the National Science Foundation (CHE-0809188 to M.J.M) and the National Institutes of Health (GM 64631 to T.C.B.) The U.S. Department of Energy, Division of Materials Sciences and Division of Chemical Sciences, supported XAS data collection at the National Synchrotron Light Source (NSLS) at Brookhaven National Laboratory. The National Institutes of Health supports beamline X3B (formerly X9B) at NSLS. Pulse radiolysis studies were carried out at the Center for Radiation Chemical Research, which is funded under Contract DE-AC02-98CH10886 with the U.S. Department of Energy. The authors also acknowledge Dr. Peter A. Bryngelson for contributing information regarding WT-NiSOD and for help in mutagenesis, and Robert W. Herbst for assistance in EPR and MS data collection.

Abbreviations

SODs	Superoxide dismutases
$\mathbf{O_2^{\bullet -}}$	Superoxide anion radical
$\mathbf{O_2}$	Molecular oxygen
$\mathbf{H_2O_2}$	Hydrogen peroxide

M	Redox-active metal
CuZnSOD	Cu, Zn containing superoxide dismutase
FeSOD	Cu, Zn containing superoxide dismutase
MnSOD	Cu, Zn containing superoxide dismutase
NiSOD	Cu, Zn containing superoxide dismutase
NHE	Normal hydrogen electrode
ACS	Acetyl coenzyme A synthase
COdH	Carbon monoxide dehydrogenase
H_2ase	Hydrogenase
MCR	Methyl coenzyme M reductase
Glx1	Glyoxalase
ARD	Acireductone dehydrogenase
DFT	Density functional theory
C2S	Cys2 to Ser mutation
C6S	Cys6 to Ser mutation
C2S/C6S	Cys2 and Cys6 to Ser mutation
Cys → Ser	Cys-to-Ser mutations
WT	Wild type
LIC	Ligation independent cloning
cam	chloramphenicol
kan	kanamycin
IPTG	Isopropyl β-D-1-thiogalactopyranoside
ESI-MS	Electrospray ionization mass spectroscopy
MW	Molecular weight
MWCO	Molecular weight cut off
BCA	Bicinchoninic acid
DTT	Dithiothreitol
ICP-OES	Inductively coupled plasma-optical emission spectrometer
SCD	Segmented-array charge-coupled device
V_e/V_0	Retention volume
T_m	Melting temperature
VP-DSC	Variable pressure differential scanning calorimeter
XAS	X-ray absorption spectroscopy
XANES	X-ray absorption near-edge spectroscopy
EXAFS	Extended X-ray absorption fine structure
EDTA	Ethylenediaminetetracetic acid

OH	Hydroxide
HCO_2^-	Formate
H_2O	Water
$CO_2^{\bullet -}$	Carbon dioxide anion radical
CO_2	Carbon dioxide
e_{aq}^-	Aqueous electron
$H^\bullet$	Hydride anion radical
$HO_2^\bullet$	Water radical
H^+	Proton
DSC	Differential scanning calorimetry
EPR	Electron paramagnetic resonance
family II PPase	family II pyrophosphatase
B. subtilis	*Bacillus subtilis*

References

1. Cabelli, DE.; Riley, D.; Rodriguez, JA.; Valentine, JS.; Zhu, H. Biomimetic Oxidations Catalyzed by Transition Metal Complexes. Meunier, B., editor. Imperial College Press; London: 1998. p. 461-508.
2. Fridovich I. Ann Rev Biochem 1995;64:97–112. [PubMed: 7574505]
3. Miller A-F, Sorkin DL. Comments Mol Cell Biophys 1997;9(1):1–48.
4. Touati, D. Oxidative Stress and the Molecular Biology of Antioxidant Defenses. Scandalios, JG., editor. Cold Spring Harbor Laboratory Press; Plainview, NY: 1997. p. 447-493.
5. Bannister JV, Bannister WH, Rotilio G. CRC Crit Rev Biochem 1987;22(2):111–180. [PubMed: 3315461]
6. Fridovich I. Ann Rev Biochem 1975;44:147–159. [PubMed: 1094908]
7. Kim EJ, Chung HJ, Suh B, Hah YC, Roe JH. Mol Microbiol 1998;27(1):187–195. [PubMed: 9466266]
8. Lee, JW.; Roe, JH.; Kang, SO., editors. Superoxide Dismutase. 2002. p. 90-101.
9. Uudsemaa M, Tamm T. J Phys Chem A 2003;107(46):9997–10003.
10. Fee, JA.; Valentine, JS. Superoxide and superoxide dismutases. Michelson, AM.; McCord, JM.; Fridovich, I., editors. Academic Press; London and New York: 1977. p. 25-28.
11. Bordo D, Matak D, Djinovic-Carugo K, Rosano C, Pesce A, Bolognesi M, Stroppolo ME, Falconi M, Battistoni A, Desideri A. J Mol Biol 1999;285(1):283–296. [PubMed: 9878406]
12. Borgstahl GE, Parge HE, Hickey MJ, Beyer WF Jr, Hallewell RA, Tainer JA. Cell 1992;71(1): 107–118. [PubMed: 1394426]
13. Lah MS, Dixon MM, Pattridge KA, Stallings WC, Fee JA, Ludwig ML. Biochemistry 1995;34(5): 1646–1660. [PubMed: 7849024]
14. Tierney DL, Fee JA, Ludwig ML, Pennerhahn JE. Biochemistry 1995;34(5):1661–1668. [PubMed: 7849025]
15. Barondeau DP, Kassmann CJ, Bruns CK, Tainer JA, Getzoff ED. Biochemistry 2004;43(25):8038–8047. [PubMed: 15209499]
16. Wuerges J, Lee JW, Yim YI, Yim HS, Kang SO, Carugo KD. Proc Natl Acad Sci USA 2004;101(23):8569–8574. [PubMed: 15173586]
17. Darnault C, Volbeda A, Kim EJ, Legrand P, Vernede X, Lindahl PA, Fontecilla-Camps JC. Nat Struct Biol 2003;10(4):271–279. [PubMed: 12627225]

18. Doukov TI, Iverson TM, Seravalli J, Ragsdale SW, Drennan CL. Science 2002;298(5593):567–572. [PubMed: 12386327]
19. Dobbek H, Svetlitchnyi V, Gremer L, Huber R, Meyer O. Science 2001;293(5533):1281–1285. [PubMed: 11509720]
20. Volbeda A, Charon MH, Piras C, Hatchikian EC, Frey M, Fontecilla-Camps JC. Nature 1995;373(6515):580–587. [PubMed: 7854413]
21. Ermler U, Grabarse W, Shima S, Goubeaud M, Thauer RK. Science 1997;278(5342):1457–1462. [PubMed: 9367957]
22. Jabri E, Carr MB, Hausinger RP, Karplus PA. Science 1995;268(5213):998–1004. [PubMed: 7754395]
23. He MM, Clugston SL, Honek JF, Matthews BW. Biochemistry 2000;39(30):8719–8727. [PubMed: 10913283]
24. Al-Mjeni F, Ju T, Pochapsky TC, Maroney MJ. Biochemistry 2002;41(21):6761–6769. [PubMed: 12022880]
25. Pochapsky TC, Pochapsky SS, Ju T, Mo H, Al-Mjeni F, Maroney MJ. Nat Struct Biol 2002;9(12): 966–972. [PubMed: 12402029]
26. Fiedler AT, Bryngelson PA, Maroney MJ, Brunold TC. J Am Chem Soc 2005;127(15):5449–5462. [PubMed: 15826182]
27. Pelmenschikov V, Siegbahn PEM. J Am Chem Soc 2006;128(23):7466–7475. [PubMed: 16756300]
28. Prabhakar R, Morokuma K, Musaev DG. J Comput Chem 2006;27(12):1438–1445. [PubMed: 16804959]
29. Jackson TA, Brunold TC. Acc Chem Res 2004;37(7):461–470. [PubMed: 15260508]
30. Miller AF. Acc Chem Res 2008;41(4):501–510. [PubMed: 18376853]
31. Rulisek L, Jensen KP, Lundgren K, Ryde U. J Comput Chem 2006;27(12):1398–1414. [PubMed: 16802319]
32. Vance CK, Miller AF. J Am Chem Soc 1998;120(3):461–467.
33. Carrasco R, Morgenstern-Badarau I, Cano J. Inorg Chim Acta 2007;360(1):91–101.
34. Miller AF, Padmakumar K, Sorkin DL, Karapetian A, Vance CK. J Inorg Biochem 2003;93(1–2): 71–83. [PubMed: 12538055]
35. Herbst RW, Guce A, Bryngelson PA, Higgins KA, Ryan KC, Cabelli DE, Garman SC, Maroney MJ. Biochemistry 2009;48(15):3354–3369. [PubMed: 19183068]
36. Fisher CL, Cabelli DE, Hallewell RA, Beroza P, Lo TP, Getzoff ED, Tainer JA. Proteins: Struct Funct Bioinf 1997;29(1):103–112.
37. Miller AF, Sorkin DL, Padmakumar K. Biochemistry 2005;44(16):5969–5981. [PubMed: 15835886]
38. Tabares LC, Cortez N, Un S. Biochemistry 2007;46(32):9320–9327. [PubMed: 17636871]
39. Allan CB, Davidson G, Choudhury SB, Gu ZJ, Bose K, Day RO, Maroney MJ. Inorg Chem 1998;37(17):4166–4167. [PubMed: 11670546]
40. Chohan BS, Shoner SC, Kovacs JA, Maroney MJ. Inorg Chem 2004;43(24):7726–7734. [PubMed: 15554637]
41. Grapperhaus CA, Darensbourg MY. Acc Chem Res 1998;31(8):451–459.
42. Shoner SC, Olmstead MM, Kovacs JA. Inorg Chem 1994;33(1):7–8.
43. Bryngelson PA, Arobo SE, Pinkham JL, Cabelli DE, Maroney MJ. J Am Chem Soc 2004;126(2): 460–461. [PubMed: 14719931]
44. Leitch S, Bradley MJ, Rowe JL, Chivers PT, Maroney MJ. J Am Chem Soc 2007;129(16):5085–5095. [PubMed: 17397155]
45. Padden KM, Krebs JF, MacBeth CE, Scarrow RC, Borovik AS. J Am Chem Soc 2001;123(6): 1072–1079. [PubMed: 11456660]
46. Webb SM. SIXpack: a graphical user interface for XAS analysis using IFEFFIT Physica Scripta 2005;T115:1011–1014.
47. Ankudinov AL, Ravel B, Rehr JJ, Conradson SD. Phys Rev B 1998;58(12):7565–7576.

48. Johnson OE, Ryan KC, Maroney MJ, Brunold TC. J Biol Inorg Chem. 2009
49. Colpas GJ, Maroney MJ, Bagyinka C, Kumar M, Willis WS, Suib SL, Baidya N, Mascharak PK. Inorg Chem 1991;30(5):920–928.
50. Bielski BH, Cabelli DE. Int J Radiat Biol 1991;59(2):291–319. [PubMed: 1671684]
51. Fridovich I. J Exp Biol 1998;201(8):1203–1209. [PubMed: 9510531]
52. Choudhury SB, Lee JW, Davidson G, Yim YI, Bose K, Sharma ML, Kang SO, Cabelli DE, Maroney MJ. Biochemistry 1999;38(12):3744–3752. [PubMed: 10090763]
53. Cowan, JA. Inorganic biochemistry: an introduction. 2. Wiley-VCH; New York: 1997.
54. Szilagyi RK, Bryngelson PA, Maroney MJ, Hedman B, Hodgson KO, Solomon EI. J Am Chem Soc 2004;126(10):3018–3019. [PubMed: 15012109]
55. Melnik M, Sramko T, Dunajjurco M, Sirota A, Jona E, Holloway CE. Rev Inorg Chem 1994;14 (1–4):1–300.
56. Rosenfield SG, Armstrong WH, Mascharak PK. Inorg Chem 1986;25(17):3014–3018.
57. Baidya N, Olmstead M, Mascharak PK. Inorg Chem 1991;30(5):929–937.
58. Marganian CA, Vazir H, Baidya N, Olmstead MM, Mascharak PK. J Am Chem Soc 1995;117(5): 1584–1594.
59. Rosenfield SG, Berends HP, Gelmini L, Stephan DW, Mascharak PK. Inorganic Chemistry 1987;26(17):2792–2797.
60. Iwig JS, Leitch S, Herbst RW, Maroney MJ, Chivers PT. J Am Chem Soc 2008;130(24):7592–7606. [PubMed: 18505253]
61. Calatayud ML, Castro I, Sletten J, Cano J, Lloret F, Faus J, Julve M, Seitz G, Mann K. Inorg Chem 1996;35(10):2858–2865.
62. Halonen P, Tammenkoski M, Niiranen L, Huopalahti S, Parfenyev AN, Goldman A, Baykov A, Lahti R. Biochemistry 2005;44(10):4004–4010. [PubMed: 15751976]
63. Niemoth-Anderson, JD.; Rodriguez, JA.; Lee, J-W.; Roe, J.; Yim, Y-I.; Cabelli, DE.; Valentine, JS.; Kang, S-O.; Maroney, MJ. Book of Abstracts. 219th ACS National Meeting; San Francisco, CA. 2000.
64. Youn HD, Kim EJ, Roe JH, Hah YC, Kang SO. Biochem J 1996;318:889–896. [PubMed: 8836134]

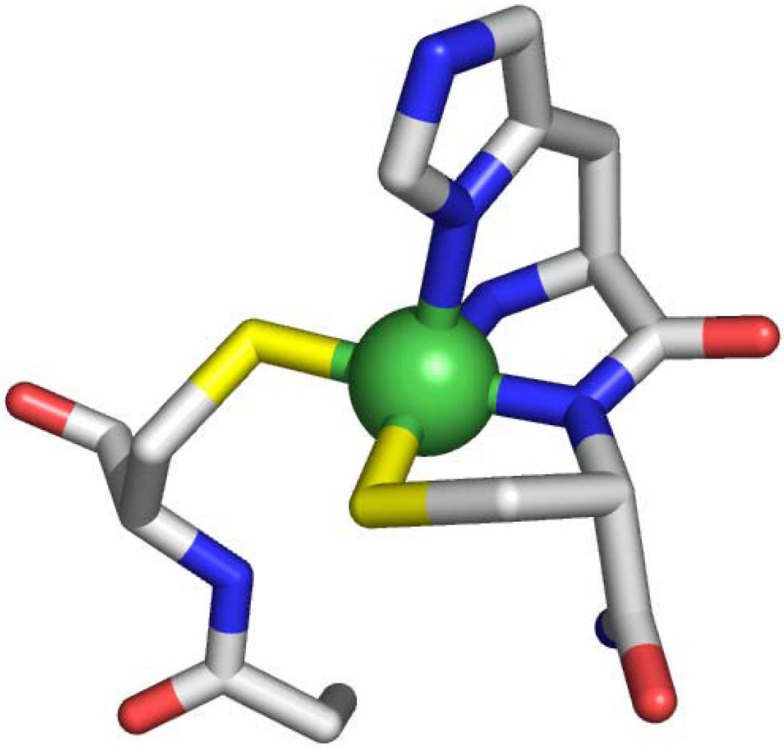

Figure 1.
Active site of NiSOD (1T6U) shown in the His-on, Ni(III)-bound state.

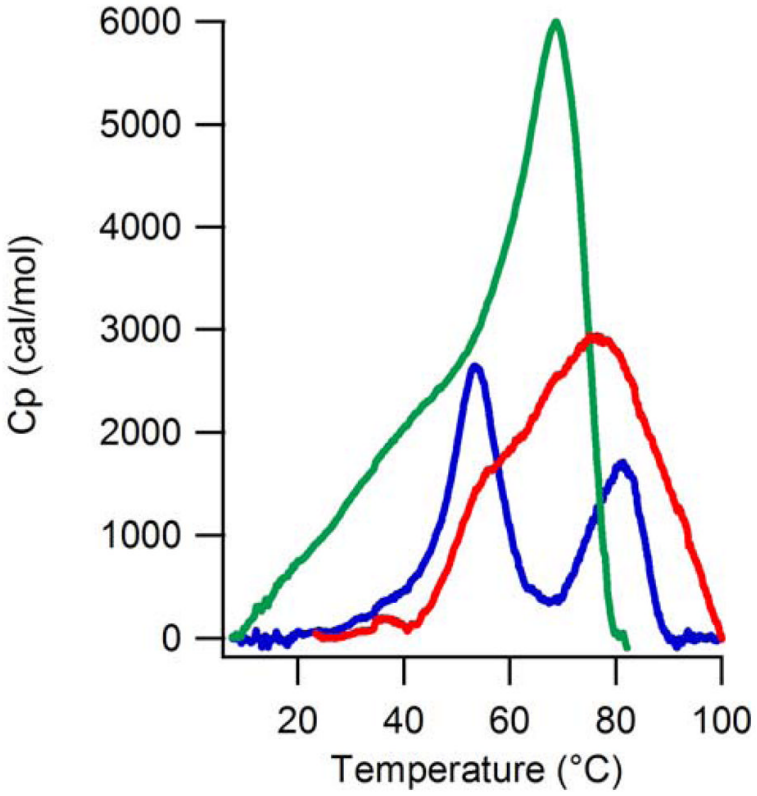

Figure 2.
DSC thermograms of C2S- (red), C6S- (green), and C2S/C6S-NiSOD (blue)

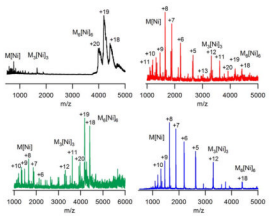

Figure 3.
ESI-MS traces obtained under non-denaturing conditions (see experimental section). WT-(black), C2S-(red), C6S-(green), and C2S/C6S-NiSOD (blue).

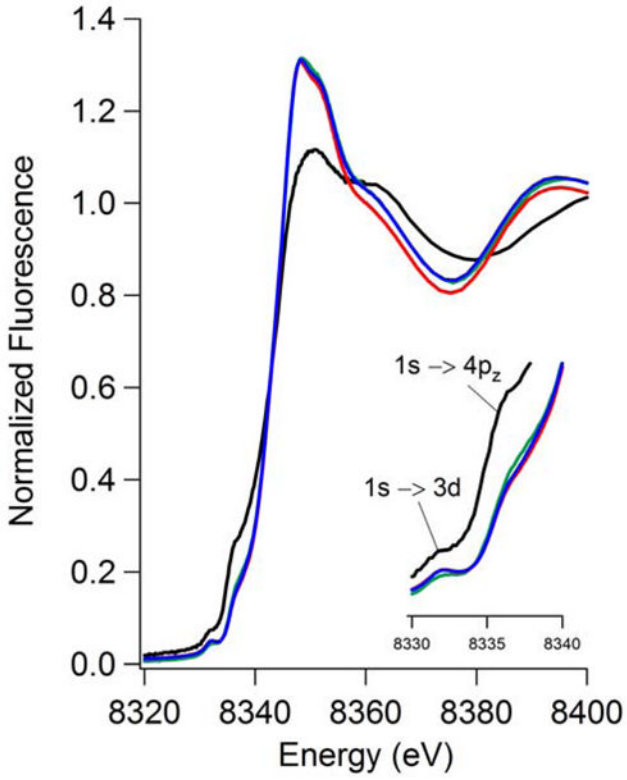

Figure 4.
Ni K-edge XANES spectra for WT- (black), C2S-(red), C6S-(green), and C2S/C6S-NiSOD(blue).

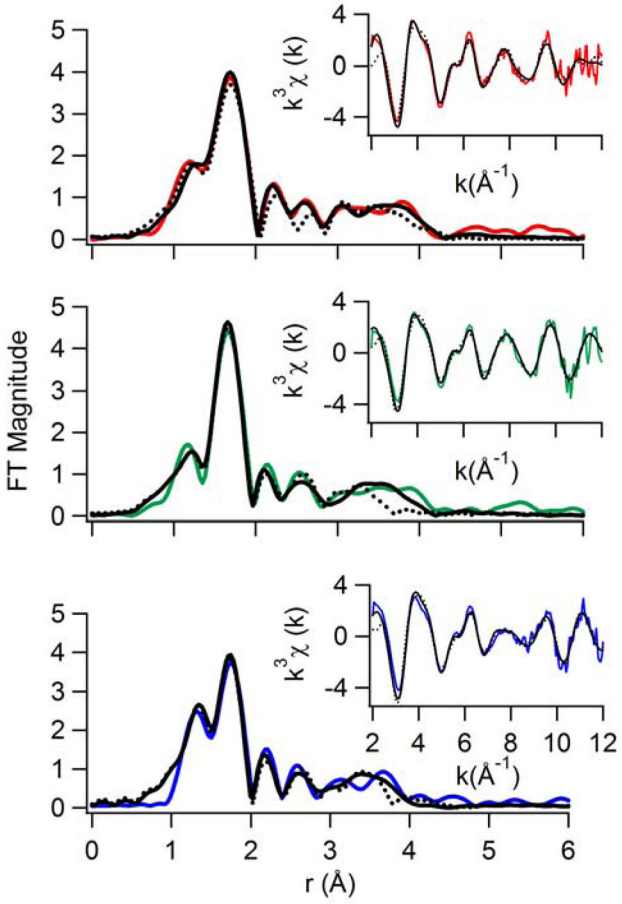

Figure 5.
EXAFS spectra (colored lines) and fits (black lines) for C2S-(red), C6S-(green), and C2S/C6S-NiSOD(blue). The dashed line indicates fits generated without an imidazole ligand and a solid line corresponds to fits including one imidazole ligand.

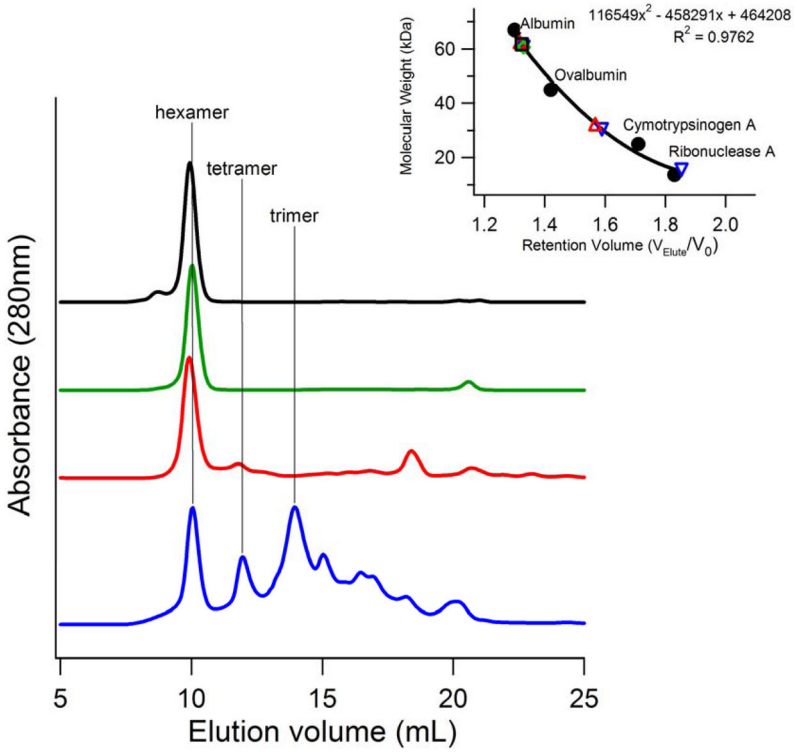

Figure 6.
Size exclusion chromatograms for WT- (black). C2S- (red), C6S- (green), and C2S/C6S-NiSOD (blue).

Table 1

Mutagenic primers for C2S-, C6S-, and C2S/C6S-NiSOD

Mutant	Forward Primer	Reverse Primer	Parental DNA
C2S-NiSOD	5′-GGTATTGAGGGTCGCCACTCCGACCTGCCTTGCG-3′	5′-AGAGGAGAGTTAGAGCCCTTTGTTAGCAGCCGG-3′	WT-NiSOD
C6S-NiSOD	5′-GGTATTGAGGGTCGCCACTGCGACCTGCCTTCCGGCGTGTACG-3′	5′-AGAGGAGAGTTAGAGCCCTTTGTTAGCAGCCGG-3′	WT-NiSOD
C2S/C6S-NiSOD	5′-GGTATTGAGGGTCGCCACTCCGACCTGCCTT-3′	5′-AGAGGAGAGTTAGAGCCCTTTGTTAGCAGCCGG-3′	C6S-NiSOD

Table 2

Characterization of Native, WT, and Cys mutants of NiSOD

NiSOD sample	MW (ESI-MS) (calc'd value)	Quaternary Structure (ESI-MS)	Ni/protein	EPR as isolated	Kinetics kcat @ pH 7.5 (× 10^9 $M^{-1}s^{-1}$)	T_m (°C)
Native (*S. seoul- ensis*)	13,192.5 (13,189.1)	hexamer	0.74	g = 2.30, 2.23, 2.01 Azz = 24.9G	1.18	88.0[b] [63] (>80)[64]
WT	18,171.2[a] (18,169.6)	hexamer	0.88	g = 2.30, 2.23, 2.01 Azz = 24.9G	0.55	84.8[b] 65.2[c]
C2S	18,152.4[a] (18,153.3)	monomer, trimer, and hexamer	0.98	Silent	0.005	76.4[b], 45.9[c]
C6S	18,153.9[a] (18,153.3)	monomer, trimer, and hexamer	0.86	Silent	0.003	68.7[b], 55.8[c]
C2S/C6S	18,137.2[a] (18,139.4)	monomer, trimer, and hexamer	0.73	Silent	0.001	53.5[b], 81.3[b]

[a]Indicates fusion protein,

[b]Heat capacity peak maximum,

[c]Heat capacity shoulder

Table 3

Size-exclusion Chromatography

NiSOD sample	Elution volume (mL)	MW (kDa)	Corrected MW (kDa)	Quaternary Structure (cal'd, kDa)
WT	9.94	61.1	79.2	Hexamer (79.2)
C2S	9.95	62.1	79.5	Hexamer (79.1)
	11.80	31.8	49.3	Tetramer (52.7)
C6S	10.02	60.1	77.6	Hexamer (79.1)
C2S/C6S	10.00	60.3	77.8	Hexamer (79.0)
	12.00	29.8	47.3	Tetramer (52.7)
	14.00	15.0	32.5	Trimer (39.5)

Table 4

XANES and EXAFS Analysis

Sample	Edge Energy (eV)	1s→3d peak area (×10^2 eV)	Geometry	N	R (Å)	σ^2 (×10^3 Å^{-2})	ΔE$_0$ (eV)	Reduced χ^2	Residual
C2S[a]	8344.9(6)	6.5(6)	spy	1N	1.83(2)	2(2)			
				2N	1.99(1)	0(2)	11(1)	8.04	0.0197
				2O	2.11(1)	1(1)			
C2S[b]				1N	1.78(2)	1(2)			
				2N	1.93(3)	0(3)	3(2)	29.74	0.0418
				2O	2.07(2)	1(2)			
C6S[a]	8344.8(6)	5.8(5)	spy	2N	1.84(1)	8(2)	8(2)	14.44	0.0342
				3O	2.04(1)	4(1)			
C6S[b]				2N	1.83(2)	7(2)	7(2)	21.93	0.0519
				3O	2.03(1)	4(1)			
C2S/C6S[a]	8345.5(2)	6.7(6)	spy	2N	1.90(1)	4(1)	11(1)	43.17	0.0508
				3O	2.08(1)	4(1)			
C2S/C6S[b]				2N	1.90(2)	4(2)	9(2)	59.40	0.0699
				3O	2.08(1)	4(1)			

[a] Includes one imidazole,

[b] Includes zero imidazole